Experimental and numerical characterization of liquid jet injected into air crossflow with acoustic forcing

Anthony Desclaux, Swann Thuillet, Davide Zuzio, Delphine Sebbane, Virginel Bodoc, Pierre Gajan

Experimental and numerical characterization of liquid jet injected into air crossflow with acoustic forcing

Anthony Desclaux[1*], Swann Thuillet[1¤], Davide Zuzio[1†], Delphine Sebbane[1], Virginel Bodoc[1], Pierre Gajan[1]

[1] Department Multi-Physics for Energetic, O.N.E.R.A.

2 Avenue Edouard Belin, 31000 Toulouse

[*]anthony.desclaux@onera.fr, [¤]swann.thuillet@onera.fr, [†]davide.zuzio@onera.fr

Keywords: liquid jet, crossflow, atomization, acoustics, multi-scale

Abstract

This paper focus on the dynamic of a spray issued from the shearing of a liquid jet injected in an air crossflow submitted to high acoustic perturbations. Experimental and numerical approaches are used. Characterization of the liquid jet close to the injection location is obtained from high speed visualizations performed with a back lighting technique. Phase Doppler Anemometry gives useful information on the spray dynamics. The phase-averaged post processing method is chosen to describe the flow oscillations during the excitation cycle. The numerical simulation is performed with the multi-scale LES approach. This method couples a multi-fluid solver for the liquid jet body with a dispersed phase solver dealing with the atomized spray. The experimental results show a swigging phenomenon of the liquid jet and the existence of velocity and concentration waves travelling downstream of the liquid jet. Coupled phenomena between the crossflow, the atomization of the liquid jet and the transport of droplets are observed, revealing different wave transport velocities. The numerical simulation is able to capture the global swinging phenomenon of the liquid jet main body as well. A very good agreement is obtained for the jet trajectories oscillations obtained either by the simulation or from the experiment during the whole excitation cycle.

Introduction

The increasing demand for civil air transportation may lead to negative environmental effects from polluting emission like NOx, soot or carbon monoxide emissions. Because of this, manufacturers try to reduce the environmental impact by modifying their engine concept. Efforts have in consequence been put into the development of advanced technologies. In particular, manufacturers developed combustion chambers operating in lean combustion regimes in order to minimize pollutant formation. These new chambers requires improved liquid injection systems to enhance the fuel/air mixing, in order to achieve fine and uniform distributions of fuel droplets. Therefore, multi-point injectors were designed. They comprised two injection zones, a pilot zone composed of a pressure atomizer in the center and a multipoint zone at the periphery. In this latter zone, the liquid fuel is injected through a set of individual liquid jets inside the swirler channels, in an atomization configuration corresponding to a Liquid Jet In a Cross Flow (LJICF).

However, systems operating in lean combustion regime may enhance the onset of combustion instabilities resulting from a coupling between the acoustic field (pressure p' and velocity fluctuation v'), and the unsteady heat release (q') from the flame. These instabilities can lead to large cyclic pressure or velocity fluctuations inside the chamber, and consequently generate significant heat transfer at the combustor walls or large amplitude vibrations of the structure. This can result in damage of the combustor or even to its destruction. In the literature, many researches deal with gas-fueled combustors in premixed or diffusion regimes in order to describe and model the phenomena concerned and determine the p' (or u') - q' relationship.

When a liquid fuel is used, the coupling between the acoustic fluctuations and the unsteady heat release involve additional phenomena such as spray atomization / transport / vaporization / combustion and their interaction with turbulence, vorticity, chemistry, and acoustics. In this way, Eckstein et al. (Eckstein et al. 2006) analyzed that, when combustion instabilities occur, the periodic velocity fluctuations inside the atomizer create a time-varying droplet size distribution, which is transported further downstream to the flame as a droplet wave. During this convection phase, the small-droplet zones produce a larger amount of fuel vapor than the large-droplet zones. As a result, an equivalence ratio wave appears which interacts with the flame to produce a periodic heat release oscillation. More recently, Apeloig et al. (Apeloig et al. 2015) studied the unsteady interaction of a kerosene spray downstream of a multi-point injector with the flame. Phase-averaged image processing obtained from planar laser-induced fluorescence (PLIF) on kerosene reveals a cyclic variation of the spatial distribution of the liquid kerosene concentration. This

phenomenon can be related to the unsteady behavior of the individual liquid jets inside of the multipoint zone when they are submitted to acoustic forcing from the air flow. Depending on the amplitude and frequency of the air velocity oscillations and the averaged momentum flux ratio q between the two fluids, the liquid jets may cyclically impact the inner or the upper wall of the injection system forming a liquid film which is re-atomized at the edge of the diffuser. Such coupling between the air crossflow and the atomization of a liquid jet was shown by Anderson et al. (Anderson, Proscia & Cohen 2001), Song and Lee (Song, Ramasubramanian & Lee 2013) and Sharma and Lee (Sharma & Lee 2018).

In the literature, many investigations of the atomization process in constant air flow were published ((Wu et al. 1997); (Sallam, Aalburg & Faeth 2013); (Broumand & Birouk 2016); (Mashayek A. 2011)). The influence of different parameters such as the moment flux ratio q ($=\rho_l V_j^2/\rho_g V_g^2$) or the Weber number We ($=\rho_g V_g^2 d/\sigma$) on the liquid behavior was demonstrated.

Therefore, the atomization regime of the liquid jet column is controlled by the Weber number. For Weber number above 110, Sallam et al. (Sallam, Aalburg & Faeth 2013) observed that a shear breakup regime is obtained. It begins by deflection of the liquid jet but with negligible distortion of the jet cross section. Wavelike disturbances appear on the upstream side of the jet as a result of Rayleigh-Taylor instabilities, which grow into ligaments along the periphery of the liquid jet. Instabilities on these last one are at the origin of droplets which break away from the liquid column to form a spray. Wu et al. (Wu et al. 1997) distinguished two atomization modes, the first on the jet surface and the second at the end of the liquid column, namely surface and column breakup. At the column breakup location the liquid jet stops to form a continuous stream (i.e. liquid column). It corresponds to the beginning of the spray. Sallam et al (Sallam, Aalburg & Faeth 2013) showed that the sizes of the ligament and droplet depend on the atomization regime and are correlated to a non-dimensional number based on the Weber number and on the liquid to gas viscosity ratio ($(\mu_l/\mu_G)(1/We)$).

Many authors observed that the jet trajectory is mainly influenced by the moment flux ratio. Nevertheless a great dispersion in the results is obtained (No 2015). This dispersion is linked to the measurement and processing techniques; the turbulence level in the jet core related to the injector geometry, the boundary layer of incoming gas flow. Wu et al investigated the influence of different parameters on the axial (y_b) and transverse (z_b) location of the jet column breakup. They observed that the ratio y_b/d is nearly independent of the moment flux ratio ($y_b/d \sim 8.06$) whereas the transverse location varied as $3.07.q^{0.53}$. Nevertheless there exist discrepancies concerning the determination of this length in the literature cause by an accurate determination of this location due to high droplets (or ligaments) density around the jet column.

The influence of an acoustic forcing greatly depends on the modulation rate defined by $\tau = u'_{rms}/\overline{U}$ and a non-dimensional time scale parameter comparing the breaking time scale of the column introduce by Wu et al ($t_b = 3.07(d/v_j)q^{0.53}$) to the oscillating period of the excitation ($T = 1/f$) Anderson et al (Anderson, Proscia & Cohen 2001), Song and Lee (Song, Ramasubramanian & Lee 2013), Sharman and Lee (Sharma & Lee 2018). For high excitation level and small time scale ratio, large oscillations of the liquid column were observed. On the opposite case Song and Lee observed negligible influence of the excitation on the jet trajectory but a periodic variation of the droplet size distribution.

In order to obtain a detailed description of the interaction between atomization and acoustic perturbations, a simplified test rig (SIGMA) was developed at ONERA, focusing on a single injection point in the form of a water liquid jet weakly turbulent into subsonic air crossflow in a confined pipe summited to an acoustic excitation. Within this paper, the experimental characterization of a Liquid Jet in an Oscillating Cross Flow (LJIOCF) atomization is presented and compared to numerical simulations using a multi-scale approach developed especially for the SIGMA test rig configuration.

The aim of this numerical simulation is to predict the effect of an acoustic perturbation of the shearing air flow on the (primary) breakup of a liquid jet. Many numerical studies ((Desjardins, Moureau & Pitsch 2008); (Gorokhovski & Herrmann 2008); (Pai, Pitsch & Desjardins 2009)) were performed with Direct Numerical Simulation (DNS), based on advanced interface methods describing the whole atomization process, from the larger to the smaller scale. However, capturing these small scales within a full chamber simulation is still out of reach. Therefore, industrial simulations of combustion chambers are based on more efficient LES (Large Eddy Simulation) simulations ((Dorey 2012); (Eyssartier 2012); (Senoner et al. 2009)). In this approach, the liquid fuel injection is performed through a direct injection of droplets at the injector nozzle. By this way, the coupling between the gas and liquid phases during the atomization process is not taken into account.

For this reason, the simulation presented in this paper uses a multi-solver approach. The numerical simulation takes in account the largest scales of the liquid primary atomization by an appropriate large-scale model; a dedicated atomization model allows then the dynamic generation of the dispersed phase; the evolution of the cloud of droplets is then taken in account by a dispersed phase approach.

First, a description of the experimental set up and methods is detailed. Then the multi-scale approach, as well as its implementation within the CEDRE code is presented. The third section concerns the main results obtained and the comparison between both approaches followed.

Experimental set up

The SIGMA experimental set up shown in Figure 1 was designed to obtain an air flow submitted to high acoustic

levels. The air flow issued from a high pressure tank was directed into a plenum placed upstream of a pneumatic loudspeaker working in the sonic regime. The mass flow rate is directly linked to the pressure and the temperature measured in the plenum with a K-type thermocouple and a gauge pressure. This system was previously calibrated and accuracy at less than 1% is obtained. The test model is connected to the pneumatic loudspeaker through a 2m long straight pipe having a 50X50 mm2 square cross section. The overall pipe length downstream of the pneumatic loudspeaker was designed, first to permit the flow development to steady conditions and then to obtain acoustic modes in the frequency range observed in combustion chambers (between 100HZ to 600 Hz). The outlet liquid jet is placed close to a velocity antinode corresponding to high air velocity fluctuations.

The test model is sketched in Figure 2. It consists in three zones. The inlet zone, 100 mm long, has the same cross section than the upstream duct. It is followed by a convergent ensuring a channel height reduction with a smooth transition without airflow separation. The third zone having a rectangular cross section (20x50 mm^2) corresponds to the test section 110 mm long. At its end, air and liquid flows exit in the room at ambient conditions. For visualization, the vertical walls of the test section are made with Perpex. A glass window is put on the top of the test section to allow the study of the liquid film generated by the impact of the liquid jet on the upper wall. A set of 7 microphone taps placed as in Figure 2 enables the acoustical characterization of the setup.

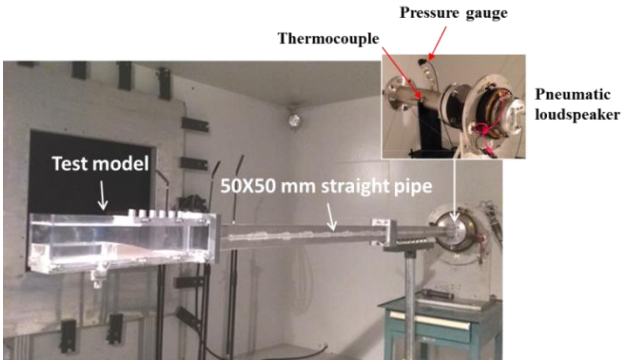

Figure 1: The SIGMA experimental set up.

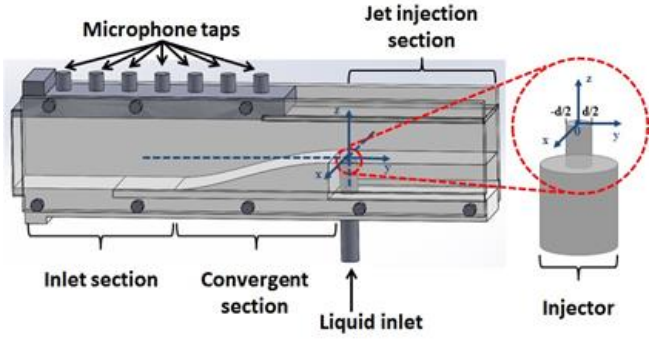

Figure 2 : SIGMA test model.

A liquid jet of water is injected vertically upwards in the symmetry plane of the test model, flush with the floor wall. The nozzle is placed 100 mm from the exit of the test section. The liquid injection system consists of a large tank, a pump, a flowmeter and a nozzle. The liquid flow rate is measured with a Coriolis Micro Mass Flow Sensor and controlled with the pump (Micropump 75211-30). Measured mass flow rate is used to calculate the jet initial velocity (u_j) at the nozzle exit. The nozzle geometry is adapted from Wu et al (Wu et al. 1997) in order to guarantee that a low liquid turbulence intensity at the jet exit. The nozzle passage has an inlet diameter of 6 mm followed by a 45° reduction to reach the specific nozzle exit diameter (d_j=2 mm). The length/diameter ratio of this last straight section is equal to 4.

Experimental methods

The experimental conditions considered for this study are summarized in Table 1. The air and liquid velocities are chosen to reproduce the main flow phenomena encountered in aeronautical aircraft engines in working conditions. The air bulk velocity is defined in the jet injection cross section.

Parameters	Values
Air flow rate [g/s]	75,7
Air bulk velocity [m/s]	63
Test liquid	Water
Liquid flowrate [l/min]	0.92-1.73
Liquid velocity [m/s]	5-11
Momentum flux ratio q [-]	7.8-17.5
Weber Number We [-]	136
Reynolds number of the air Re_{air} [-]	~21500
Airflow modulation frequency [Hz]	177

Table 1 : Experimental conditions.

Different techniques were used to analyze the flow behavior. The acoustic field was identified from the processing of sound pressure signals delivered by a microphone located at the different longitudinal places on the upper wall of the test model. Using a 1D model and the experimental determination of outlet acoustic condition, the velocity and the pressure wave, amplitude distributions were determined. A Phase Doppler Anemometry (PDA) system from DANTEC was used to characterize both the air flow field and the spray. For the air velocity field, the flow is seeded with DHES particles injected far upstream of the test section.

High speed flow visualization were recorded from a black and white Phantom camera V341 coupled with a pulsed back lighting using two Dedocoo lamps. The frame rates varied between 800 and 10000 frames/s in order to capture flow features with different characteristic times. The integration time was kept generally below 50 µs in order to freeze the motion of the liquid column and the droplets. Multiple videos were recorded for each test

condition. Dedicated software was developed to analyze the liquid behavior.

Phase-averaged analysis was applied to process the signals and video records. The acoustic velocity signal at the location of the liquid jet exit was used as reference signal. On each measurement point, the velocity and size of 10^6 individual droplets were phase averaged for 90 phases with a step of 4°. To characterize the liquid jet behavior 38428 instantaneous images were considered with a phase angle step of 10° and a bandwidth of 4°.

Numerical approach

The numerical simulation is performed with the multi-scale LES approach of the CEDRE code (Blanchard 2016). This method couples a multi-fluid solver for the liquid jet main body with a dispersed phase solver dealing with the atomized spray. The acoustic perturbation is imposed as a fluctuating air inflow condition, the resulting acoustic velocity and pressure fields having been validated against a theoretical model.

The multi-fluid model is based on finite volume discretization of Navier-Stokes conservation equation for both liquid and gas. The hypothesis of local mechanical equilibrium imposes that the two fluids have the same velocity and pressure within the given cell. The considered fluids are water and air, thus two phases consisting at single species are used without any loss of generality. No explicit interface reconstruction is performed; the interface is therefore implicitly defined by smooth variations of the phase's volume fractions. Since two-fluid model should simulate the main liquid body of the LJICF, surface tension terms are taken in account by a generalized Continuum Surface Stress ((Lafaurie et al. 1994); (Desjardins, Moureau & Pitsch 2008)) formulation.

Once the interface became too smeared, the coupling with the dispersed phase solver is activated and the liquid mass directly converted into droplets. The numerical resolution of the multi-fluid model relies on a Finite Volume approach on general unstructured meshes. The time discretization is based on an explicit RK2 scheme. A second-order MUSCL scheme is used to achieve robust second order space accuracy. Thermodynamic closure laws are considered for each phase: perfect gas and weakly compressible liquid (Dutoya & Matuszewski 2011). The coupling source terms include classical momentum and energy two-way approach effects, as well as the multi-solver interactions.

The dispersed phase model is based on a statistical Boltzmann-like density function conservation equation. Its discretization is performed with a Lagrangian approach. This model simulates the behavior of liquid spherical particles suspended into a carrying phase; the volume of the droplets is considered negligible.

The only considered external forces acting on the particles are drag and gravity. Drag force $\boldsymbol{F_{p,D}}$ is given by a Schiller-Naumann correlation (Mashayek A. 2011). The dispersed phase model is coupled in a two-way approach with the two-fluid model for modelling the mechanical (drag) and thermal exchanges as well as the mass transfer.

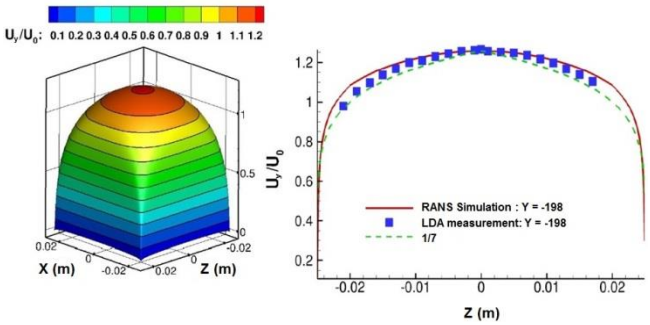

Figure 3 : Air crossflow velocity field imposed to the inlet boundary condition.

To limit the computing cost, the computational domain was limited to the test model (Figure 2). To be representative of the experiments, different boundary conditions need to be imposed. The first concerned the inlet air velocity distribution. A RANS simulation of the flow inside of the upstream square channel was performed. The axial velocity obtained at the end of the channel is compared to the experimental measurements in Figure 3. The second condition concerned the acoustic impedance and the amplitude of the excitation imposed at the inlet of the computing domain. A non-reflecting condition was used and the amplitude was fixed to obtain the same excitation level at the liquid jet injection location.

Results and Discussion

In this section, a cross-comparison is first performed to validate both the numerical model and the method used to analyze the experimental data. The air flow characterization and its numerical validation are first presented for the steady and forced flow conditions. Then, the numerical simulation of the LJICF obtained without acoustic forcing is compared to experimental results.

Finally, the characterization of the forced atomization is presented and analyzed from a detailed data base, obtained by both experiment and numerical simulations.

Experimental and numerical cross-comparison

Aero-acoustic characterization

For this characterization no liquid was injected. Using microphone and PDA measurements, the measured longitudinal distribution of the pressure and velocity waves amplitudes are compared to theoretical predictions given by a 1D model based on the Helmholtz equations (Figure 4). It can be observed that the experimental data upstream of the test section are in very good accordance with the 1D model, but diverge farther downstream. Acoustic pressure up to 1900 Pa (160 dB) is measured upstream of the convergent section while the r.m.s. velocity fluctuation is around 6.5 m/s at the liquid jet exit location, which corresponds to a modulation level of 10% with respect to the local air bulk velocity.

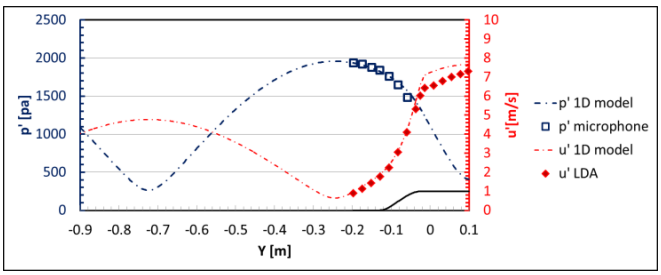

Figure 4 : Longitudinal distribution of the acoustic pressure and velocity inside of the experimental set-up.

In Figure 5, the longitudinal distribution of the amplitude and the phase of the velocity signal obtained from the simulation are successfully compared to experiments.

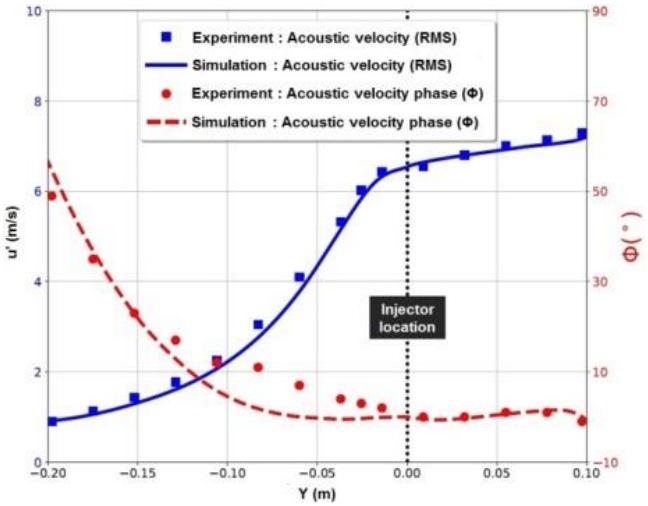

Figure 5 : Experimental and numerical comparison of the acoustic velocity field along the test model.

Characteristics of a liquid jet in a steady flow condition

In this first step, the experimental and numerical results obtained in steady air flow conditions are compared.

Following the classification given by Sallam et al. (Sallam, Aalburg & Faeth 2013), the primary breakup regime used in this study always corresponds to *shear breakup mode* characterized by a large Weber number, *We>110)*.

Examples of instantaneous and averaged images obtained from the two approaches are shown in Figure 6. The experimental visualization shows that the liquid jet bends towards the leeward direction and impacts the upper wall of the channel, forming a liquid film. Waves appearing along the surface of the liquid column are amplified by the shearing air, leading to both column and surface breakup processes and generating different liquid structures like ligaments and droplets. The simulations capture the main body behavior by the multi-fluid model as well as the subsequent cloud of droplets. As no explicit interface reconstruction is performed, the gas/liquid interface is, in this case, identified by the iso liquid volume fraction α_l=0.5. The main body shows the expected downwind bending; the jet shape flattens as it approaches the breakup point. Near this location, longitudinal instabilities can be observed, leading to a periodical release of liquid blobs which, in turn, undergo further breakup up to the formation of droplet clusters. It seems evident that the liquid body topology and position deeply affects the spray generation, which is the main objective of the multi-scale approach.

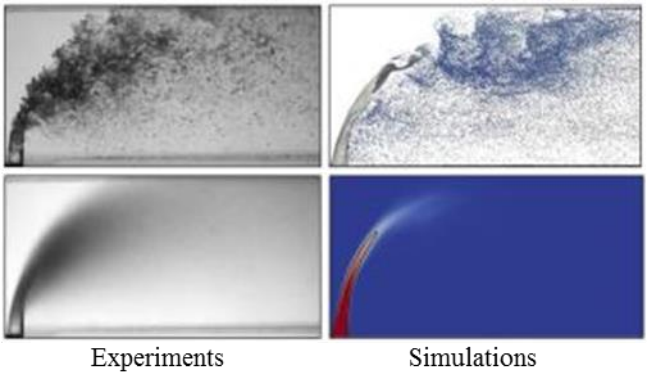

Figure 6 : Instantaneous (top) and averaged (bottom) visualization of liquid jet injected in cross flow obtained from experiments and simulations.

In order to compare the results in greater details, the jet trajectory obtained from each data base was extracted from averaged images. It is defined as the outer envelope detected from an image-processing technique. Similar post-processing methods were used in order to minimize the uncertainty. In both case this extraction is based on a thresholding method. Tests performed on numerical and experimental images show that the threshold level has a weak influence on the obtained jet trajectory. For simulations, the threshold corresponds to a liquid volume fraction α_l equal to 0.5.

Figure 7 shows a very good agreement between the jet trajectory obtained by the simulation and the experiment, especially in the column trajectory. Near the breakup region, small discrepancies can be observed.

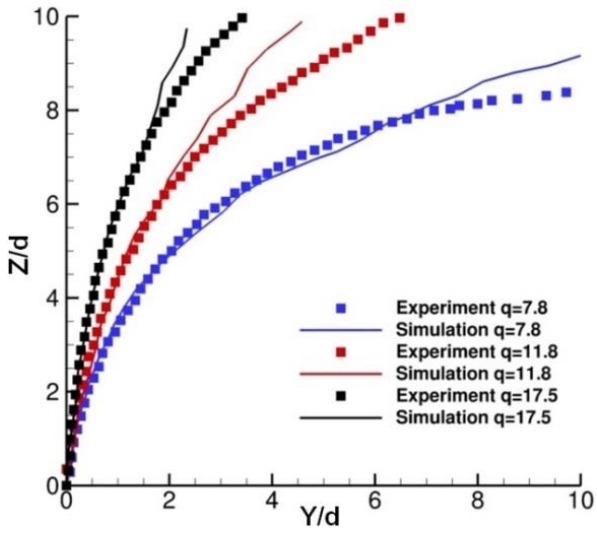

Figure 7 : Comparison of the liquid jet trajectory at various momentum ratios (*q*).

The simulation tool gives new input to analyze the influence of other parameters, like the liquid conditions at the jet outlet and the flow confinement on the jet trajectory. It is shown that when the channel cross section is reduced, the aerodynamic force applied on the jet column increases, causing a greater deflection of the jet. Simulations performed with different liquid velocity profile at the jet outlet reveal that a higher jet penetration is obtained with a Poiseuille profile compared to the uniform velocity distribution.

Characteristics of a liquid jet in a forced flow condition

This section focuses on the characteristics of a confined liquid jet injected into modulated crossflow. Figure 8 shows instantaneous shadowgraph visualizations of the jet for different phases of the air velocity oscillation. A periodic swinging phenomenon of the liquid column is observed linked to a cyclic droplet atomization from the jet column. This observation is valid only for a modulation rate above 10%. It was also shown that the liquid column breakup process is piloted by the swinging phenomenon of the liquid column. Unlike the steady crossflow configuration, the impact of liquid jet on the upper wall is cyclical and most of the ligaments and droplets induced by the column breakup process are directly carried away by the crossflow without impacting the upper wall. The numerical simulation is able to capture the global swinging phenomenon of the liquid jet main body and shows a droplets periodic release at column breakup location as well (Figure 9).

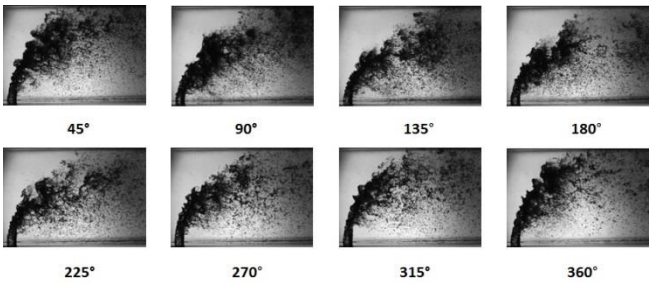

Figure 8 : Instantaneous frame sequence showing the effect of the air-crossflow modulation on the liquid jet referred to the acoustic disturbance phase.

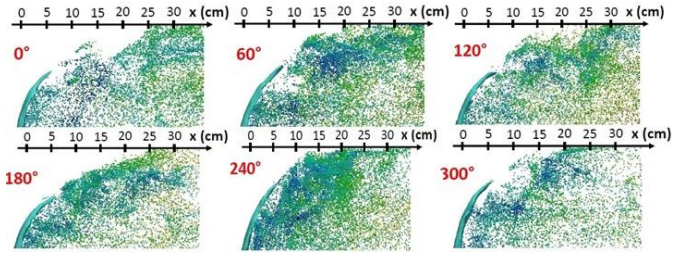

Figure 9 : Instantaneous liquid and particles fields showing the effect of the air-crossflow modulation on the liquid jet referred to the acoustic disturbance phase for the simulation.

In order to characterize the local jet behavior under crossflow modulation, a statistical power spectral analysis was performed on sequences of instantaneous visualization frames, obtained both by the experiment and the numerical simulation. It is shown that the oscillations and the breakup of the liquid column respond to the acoustic forcing. The same conclusion can be drawn for the other features of the two phase flow.

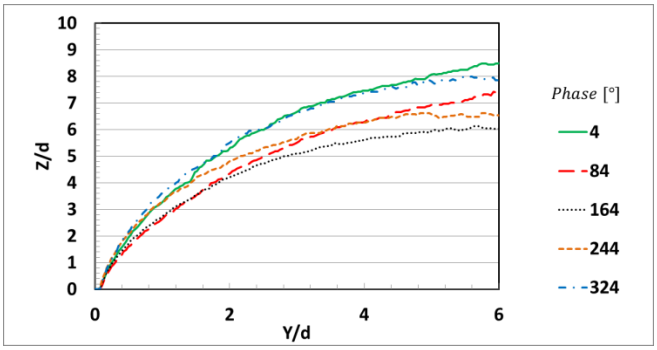

Figure 10 : Liquid jet trajectory according to the air flow acoustic velocity phase at the jet exit location, *q=7.8*, *We=136* and *f=177 Hz*.

In Figure 10 the phase-averaged oscillation of the liquid jet trajectory during the excitation cycle, obtained from the experimental data base, is shown. As indicated before, the reference phase used to process the visualizations corresponds to the air velocity signal measured at the jet outlet position. It was observed that the jet penetration height reaches its maximum position during a phase ranging from -20° and 10°. The liquid jet then bends towards the floor up-to the phase range of 160°-180°, and finally straightens back. To interpret this result, it is necessary to compare the observed trajectory movement with the reference air velocity signal. A quasi-static response of the jet would imply a phase delay of 180° between the two signals. Indeed, the minimum and the maximum jet penetration would correspond respectively to the maximum (90°) and the minimum (270°) of the air velocity signal. Therefore the liquid column responds with a phase delay of approximately 90° (Figure 11). This phenomenon is due to the inertia of the liquid jet induced by its mass.

The two most interesting points to analyze in the final spray induced by the atomization of the liquid jet are the phase delay corresponding to the column breakup and the liquid deposition on the upper wall. Figure 11 illustrates the evolution of the coordinates of the end of liquid jet as function of the phase of the acoustic disturbance. The results show that the column fracture occurs for phase ranged from 135° to 145° at the beginning of the deceleration of the air flow, as well as the maximum deflection of the liquid jet (Figure 11). The liquid deposition linked to the impact of the jet on the upper wall is observed starting from 315°- 325° up to the breakup phase. The rupture location is around $7d$ downstream of the jet inlet and $6d$ above the floor. When compared to the steady flow results (presented in the previous section), it can be concluded that the acoustic forcing does not modify

significantly the location of the liquid column breakup, but imposes a cyclic droplet ejection in the air flow with a phase delay of 45°-55° with respect to the maximum of the air velocity fluctuations.

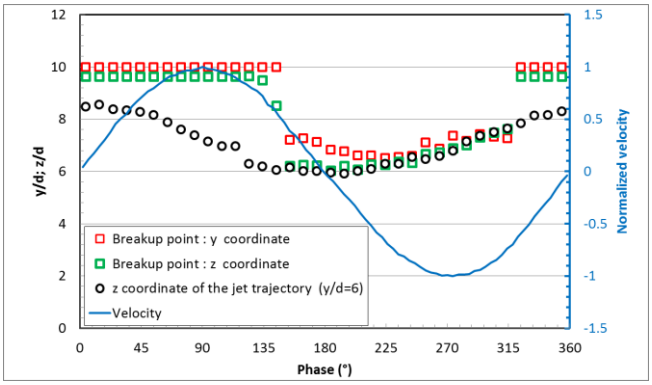

Figure 11 : Jet response as function of the acoustic disturbance phase.

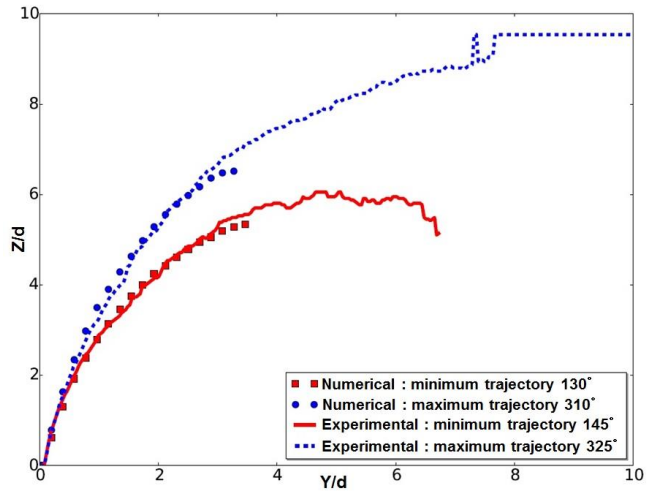

Figure 12 : Comparison between experimental and numerical maximum and minimum jet trajectories.

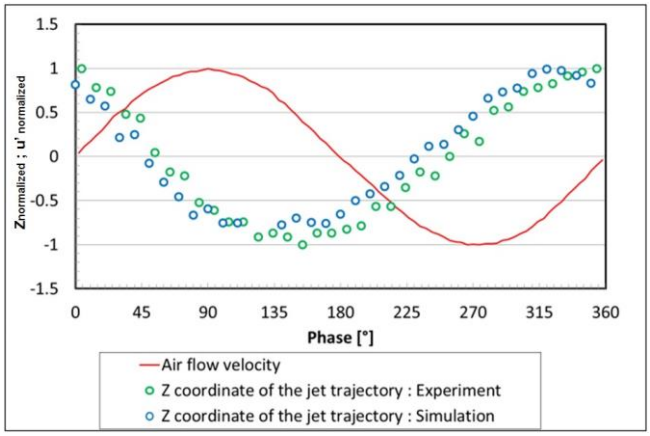

Figure 13 : Evolution of normalized trajectories heights obtained from experiment and simulation at $y/d = 2.8$.

Figure 12 compares the jet trajectory envelops obtained from experiments or simulation. The z coordinate oscillation of the jet trajectory at a fixed $y/d = 2.8$ is shown in Figure 13. These results show that the same behavior is obtained with the two approaches. In particular, the maximum and the minimum penetration heights are in very good agreement. However, a phase delay around 15° is observed between experimental and numerical trajectories. The signal obtained from simulation shows a slight phase lead compared to the experiment. This phase difference may have two origins. The first is related to the difficulty encountered in correctly estimating local drag force fluctuations when part of the liquid mass of liquid is transferred from the continuous structure of the liquid jet to droplets; this leads to a poor prediction of the force exerted by the air on the liquid jet. In parallel, an underestimation of the rupture length of the jet column induces a modification of the inertial response of the jet. As it is, it seems difficult to separate these two effects.

Characterization of the spray into modulated crossflow

The PDA technique was applied to study in more details the behavior of the spray issued from the liquid jet atomization, in the duct symmetry plane ($x/d = 0$) 15 mm above the floor ($z/d = 7.5$). The mean droplet size is around $40\mu m$ for the D_{10} and $77\mu m$ for the D_{32}.The droplet velocity distribution for droplets around $40\mu m$ are then compared to the simulation (Figure 14).

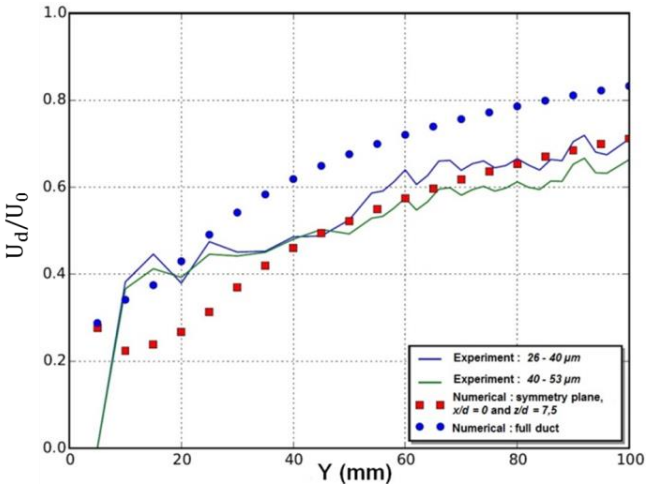

Figure 14 : Spatial distribution of the mean longitudinal droplet velocity downstream of the jet injection point.

The results show the droplets acceleration as they travel downstream in the duct. Their velocity reaches a maximum value at the end of the test model. Nevertheless, due to their large size, the droplet velocity does not reach the air velocity. Very good agreement is obtained between the two data sets from $y/d = 20$ up to the end of the duct. Nevertheless, a significant difference is observed near the jet injection location. This difference is most probably due to the difficulties for numerical simulation to accurately estimate the droplet initial velocity within the atomization model. Despite that initial underestimation, the particle drag force model provides a good estimation of the droplets velocity further downstream.

The horizontal profiles of the droplet velocity measured along the x axis for different droplet sizes are plotted in Figure 15. These curves reveal the wake effect induced by the jet body. Similar results were obtained from simulations.

Phase averaged processing of the PDA data set indicates that the spray formed consists of droplet packets moving from the jet to the channel outlet. At different locations, the phase dependence of two main parameters were analyzed; the droplet velocity and the number of particle$N$. This last one was used to compute on each location $\boldsymbol{\mathcal{M}}$ and a given phase ϕ a dimensionless number representative of the instantaneous droplet concentration:

$$\langle\chi\rangle(\boldsymbol{\mathcal{M}},\phi) = \frac{N(\boldsymbol{\mathcal{M}},\phi)}{N_T(\boldsymbol{\mathcal{M}})}$$

Typical signal evolutions along the y coordinate of these two parameters are shown in Figure 16 and Figure 17.

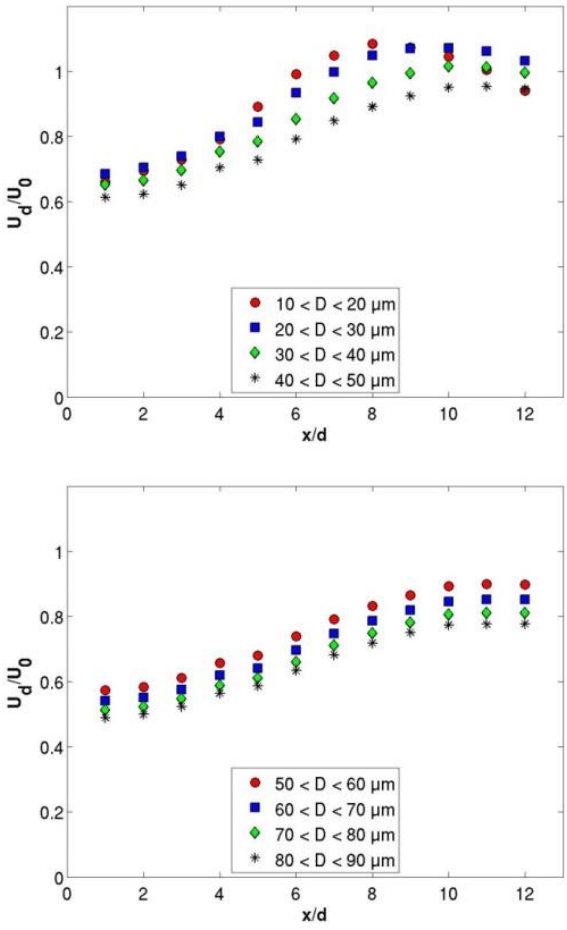

Figure 15 : Droplet velocity distribution along the x axis (horizontal) ($\frac{y}{d} = 40$; $\frac{z}{d} = 7.5$).

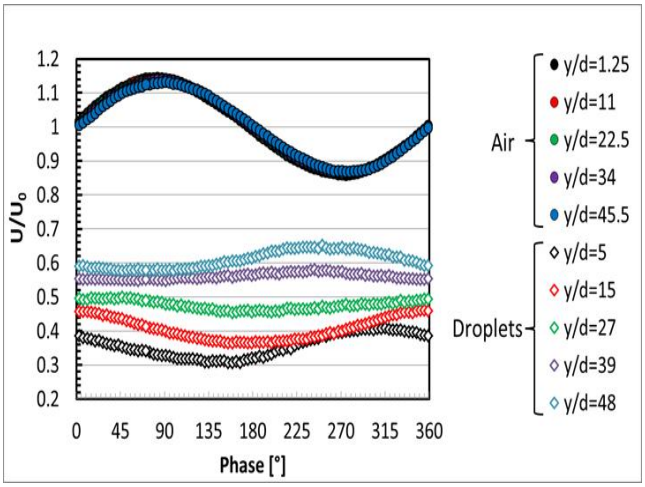

Figure 16 : Phase averaged droplet velocity signal along the y axis ($\frac{x}{d} = 0$; $\frac{z}{d} = 7.5$).

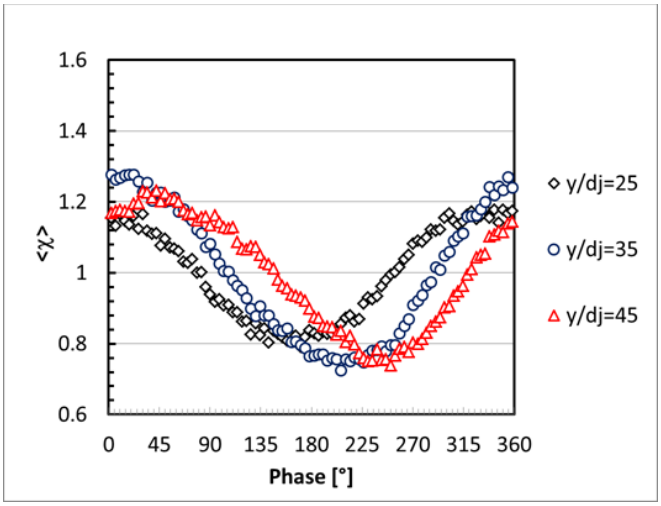

Figure 17 : Phase averaged $\langle\chi\rangle$ signal along the y axis ($\frac{x}{d} = 0$; $\frac{z}{d} = 7.5$).

While almost no phase shift is observed for the air velocity signal in function of the distance, a significant phase shift is observed on the droplet velocity signal. The convective velocity computed from the phase shift is equal to 0.45 U_0

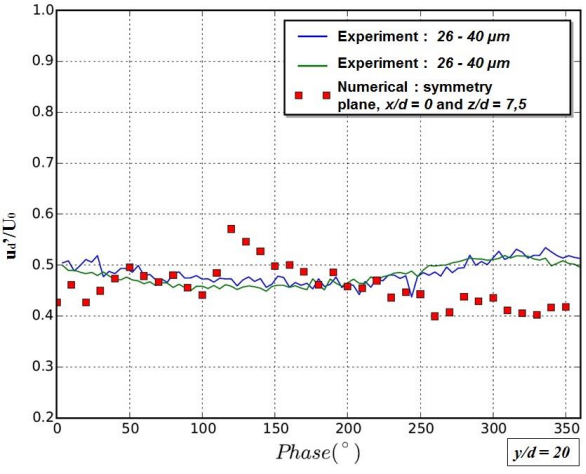

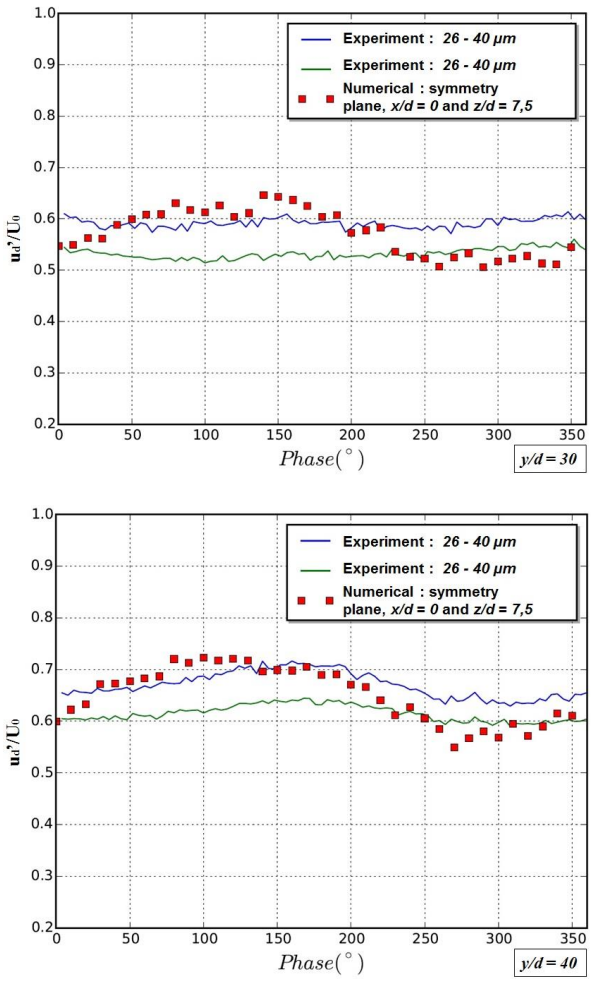

Figure 18 : Cyclic behavior of the spray downstream of the liquid jet exit (z/d=7.5). (Experimental and numerical simulation).

However, only a small phase shift is observed from numerical results (Figure 18). An estimation of this phase shift indicates a phase angle around 20° every 20 mm, and thus a maximum phase shift around 80° between the jet exit location *(y/d=10)* and the end of the duct *(y/d=50)*, compared to phase shift around 180° from experimental analyses.

Conclusions

The aim of this work is to analyze the capability of an industrial simulation approach used to predict the unsteady liquid flow phenomena encountered in industrial liquid-fueled combustion chambers with respect to the acoustic field. The simulation approach couples a multi-fluid solver for the liquid jet main body with a dispersed phase solver dealing with the atomized spray. An experimental setup reproducing the main mechanisms encountered in and downstream from an actual injection system was defined. It consists in a liquid jet sheared by an air cross flow subjected to acoustic forcing. The boundary conditions for the air and liquid flow and the acoustic field were characterized. Flow visualizations and PDA measurements were applied both in steady and forced flow conditions. Phase-averaged processing synchronized on the air velocity signal measured at the liquid jet injection point was applied on the different data bases.

The results show that the flow simulation correctly reproduces the unsteady liquid body behavior. In particular, the amplitude and phase of the oscillations of the jet trajectory induced by the acoustic forcing are in good agreement with the experimental observations. The spray behavior downstream of the liquid jet breakup is also well reproduced on averaged. This concerns the droplet acceleration. Nevertheless, the propagation of droplets packets observed experimentally was not obtained with the simulation tool. The origin of this discrepancy can be due to the atomization model used to couple the two solvers. To improve the coupling method, further work based on DNS tools is currently under way at ONERA.

Acknowledgments

This project was performed from the ONERA project SIGMA on combustion instabilities. The authors want to thank the people who participated in the realization of the tests.

References

Anderson, TJ, Proscia, W & Cohen, JM 2001, 'Modulation of a Liquid-Fuel Jet in an Unsteady Cross-Flow', *ASME Turbo expo 2001*, New, Orleans, Louisiana, <http://dx.doi.org/10.1115/2001-GT-0048>.

Apeloig, JM,d'Herbigny, F.X, Simon, F, Gajan, P, Orain, M & Roux, S 2015, 'Liquid-Fuel Behavior in an Aeronautical Injector Submitted to Thermoacoustic Instabilities', *Journal of Propulsion and Power*, vol 31, pp. 309-319, <https://doi.org/10.2514/1.B35290>.

Blanchard, G, Zuzio, D & Villedieu, P 2016, 'A large scale multi-fluid/dispersed phase approach for spray generation in aeronautical fuel injectors', *ICMF 2016*, FLORENCE, Italy, <https://hal.archives-ouvertes.fr/hal-01441814>.

Brackbill, JU, Kothe, DB & Zemach, C 1992, 'A continuum method for modeling surface tension', *Journal of Computational Physics*, vol 100, pp. 335-354, <http://www.sciencedirect.com/science/article/pii/0021999192902 40Y>.

Broumand, M & Birouk, M 2016, 'Liquid jet in a subsonic gaseous crossflow: Recent progress and remaining challenges', *Progress in Energy and Combustion Science*, vol 57, pp. 1-29, <http://www.sciencedirect.com/science/article/pii/S0360128516300235>.

Desjardins, O, Moureau, V & Pitsch, H 2008, 'An accurate conservative level set/ghost fluid method for simulating turbulent atomization', *Journal of Computational Physics*, vol 227, pp. 8395-8416, <http://www.sciencedirect.com/science/article/pii/S0021999108003112>.

Dorey, L-H 2012, 'Modelling of combustion, soot formation and radiative transfer coupled phenomena in gas turbine combustion chambers', Theses, Ecole Centrale Paris.

Dutoya, D & Matuszewski, L 2011, 'Thermodynamics in CEDRE', *AerospaceLab*, pp. p. 1-11, <https://hal.archives-ouvertes.fr/hal-01181237>.

Eckstein, J, Freitag, E, Hirsch, C & Sattelmayer, T 2006, 'Experimental Study on the Role of Entropy Waves in Low-Frequency Oscillations in a RQL Combustor', *Journal of Engineering for Gas Turbines and Power*, vol 128, pp. 264-270, <http://dx.doi.org/10.1115/1.2132379>.

Eyssartier, A 2012, 'LES of two-phase reacting flows: stationary and transient operating conditions', Ph.D. dissertation, CERFACS.

Gorokhovski, M & Herrmann, M 2008, 'Modeling Primary Atomization', *Annu. Rev. Fluid Mech.*, vol 40, pp. 343-366, <https://doi.org/10.1146/annurev.fluid.40.111406.102200>.

Lafaurie, B, Nardone, C, Scardovelli, R, Zaleski, S & Zanetti, G 1994, 'Modelling Merging and Fragmentation in Multiphase Flows with SURFER', *Journal of Computational Physics*, vol 113, pp. 134-147, <http://www.sciencedirect.com/science/article/pii/S0021999184711235>.

Le Touze, C, Murrone, A & Guillard, H 2015, 'Multislope MUSCL method for general unstructured meshes', *Journal of Computational Physics*, vol 284, pp. 389-418, <http://www.sciencedirect.com/science/article/pii/S0021999114008493>.

Mashayek A., AN 2011, 'Atomization of a Liquid Jet in Crossflow', Handbook of Atomization and Sprays.

No, S-Y 2015, 'A Review on Empirical Correlations for Jet/Spray Trajectory of Liquid Jet in Uniform Cross Flow', *International Journal of Spray and Combustion Dynamics*, vol 7, pp. 283-313, <https://doi.org/10.1260/1756-8277.7.4.283>.

Pai, M, Pitsch, H & Desjardins, O 2009, 'Detailed Numerical Simulations of Primary Atomization of Liquid Jets in Crossflow', *47th AIAA Aerospace Sciences Meeting*, American Institute of Aeronautics and Astronautics, <https://doi.org/10.2514/6.2009-373>.

Refloch, A, Courbet, B, Murrone, A, Villedieu, P, Laurent, C, Gilbank, P, Troyes, J, Tessé, L, Chaineray, G, Dargaud, JB, Quémerais, E & Vuillot, F 2011, 'CEDRE Software', *AerospaceLab*, pp. p. 1-10, <https://hal.archives-ouvertes.fr/hal-01182463>.

Sallam, KA, Aalburg, C & Faeth, GM 2013, 'Breakup of Round Nonturbulent Liquid Jets in Gaseous Crossflow', *AIAA Journal*, vol 13, pp. 64-73, <https://doi.org/10.2514/1.3749>.

Senoner, JM, Sanjosé, M, Lederlin, T, Jaegle, F, García, M, Riber, E, Cuenot, B, Gicquel, L, Pitsch, H & Poinsot, T 2009, 'Eulerian and Lagrangian Large-Eddy Simulations of an evaporating two-phase flow', *Comptes Rendus Mécanique*, vol 337, pp. 458-468, <http://www.sciencedirect.com/science/article/pii/S1631072109000667>.

Sharma, A & Lee, JG 2018, 'DYNAMICS OF NEAR-FIELD AND FAR-FIELD SPRAY FORMED BY LIQUID JET IN OSCILLATING CROSSFLOW', *Atomization and Sprays*, vol 28, pp. 1-21.

Song, J, Ramasubramanian, C & Lee, JG 2013, 'Response of Liquid Jet to Modulated Crossflow', *Proceedings of ASME Turbo Expo 2013*, San, Antonio, USA, <http://dx.doi.org/10.1115/GT2013-95726>.

Wu, P-K, Kirkendall, KA, Fuller, RP & Nejad, AS 1997, 'Breakup Processes of Liquid Jets in Subsonic Crossflows', *Journal of Propulsion and Power*, vol 31, pp. 309-319, <https://doi.org/10.2514/2.5151>.